

## CHAPTER 5

### Results and Discussion

In this Chapter, the experimental and numerical results obtained for slag formation and deposition are presented. The experimental results consist of the coal, ash, and slag characterization. Effect of calcium in ash was discussed on slag formation and deposition. Also, the numerical results include the predictions of slag formation and deposition.

#### 5.1 Characterization of Real Slag

##### 5.1.1 Microstructural Feature and Chemical Composition

SEM was used to examine the surface morphology of these slag samples. The SEM images of slag a, b, c, and d are presented in Table 5.1. Although the macroscopic appearances of the collected slag looked different, the characteristics of the surface of the SEM analysis with any random two samples indicated that they were not different. The majority of the crystal surfaces were agglomerates of particle-like clay and irregular granules stacked together.

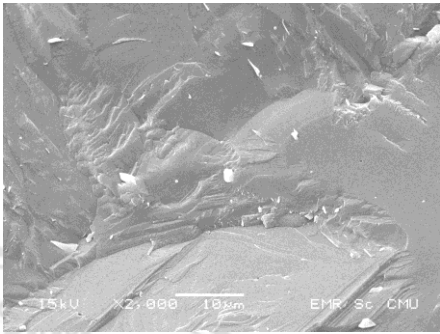
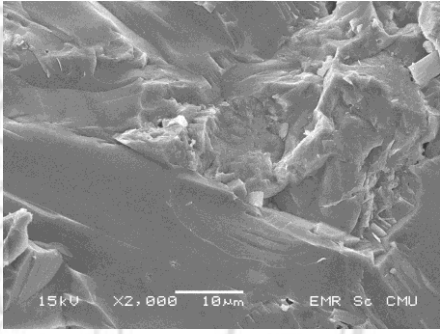
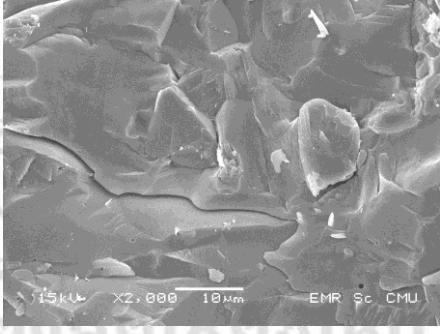
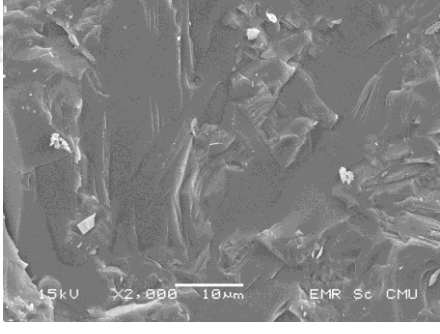
Elemental identification analyses of the samples were obtained by EDS. The results are shown in Table 5.2. The slag samples have an abundance of oxygen, aluminum, silica and calcium, which were probably quartz ( $\text{SiO}_2$ ) (Luxsanayotin *et al.*, 2010; Van Dyk *et al.*, 2009; Van Dyk, 2006), anorthite ( $\text{CaAl}_2\text{Si}_2\text{O}_8$ ) (Fernandez-Turiel *et al.*, 2004; Li *et al.*, 2011),

mullite ( $\text{Al}_6\text{Si}_2\text{O}_{13}$ ) (Li *et al.*, 2011), gehlenite ( $\text{Ca}_2\text{Al}_2\text{SiO}_7$ ) (Li *et al.*, 2011), kaolinite ( $\text{Al}_2\text{Si}_2\text{O}_7$ ) (Fernandez-Turiel *et al.*, 2004; McLennan *et al.*, 2000; Li *et al.*, 2011) and calcium oxide (CaO) (Querol *et al.*, 1995). Quartz and kaolinite are major mineral phases of coal during combustion in a large power station; and quartz, mullite and calcium oxide are major inorganic phases in slag (Querol *et al.*, 1995). The chemical reaction during the combustion of mullite and calcium oxide produces anorthite at 950°C. The reaction between anorthite and calcium oxide is gehlenite, according to Eqs. (5.1) and (5.2) (Li *et al.*, 2011). Iron, magnesium and potassium were also found. These are iron alumino-silicate ( $\text{FeO}+\text{SiO}_2+\text{Al}_2\text{O}_3$ ) (McLennan *et al.*, 2000; Li *et al.*, 2011) and siderite ( $\text{FeCO}_3$ ) (Van Dyk, 2006; McLennan *et al.*, 2000; Agraniotis *et al.*, 2009 a.; Ram *et al.*, 1995). Inorganic elements, Ca, and Mg – dissolved salts in the pore waters of coal, may have lower melting points (Li *et al.*, 2011).



The chemical composition of slag is given in Table 5.3. All of the samples were enriched in CaO,  $\text{SiO}_2$ ,  $\text{Al}_2\text{O}_3$  and  $\text{Fe}_2\text{O}_3$ . This result was in accord with the EDS analysis. However, MgO content was not disregarded. Acidic oxides (CaO,  $\text{Fe}_2\text{O}_3$ ,  $\text{Na}_2\text{O}$ , MgO) in the slag were higher than those in the ash, while the element in basic oxide ( $\text{Al}_2\text{O}_3$ ) was a smaller amount. The reasons for these results may be attributed to the decomposition, evaporation, transformation and interaction that occurred during the transformation of combustion ash particles to slag (Song *et al.*, 2009 a.).

Table 5.1 Microstructural Feature of real slag samples

Sample	Surface morphology
a	
b	
c	
d	

ลิขสิทธิ์มหาวิทยาลัยเชียงใหม่  
Copyright © by Chiang Mai University  
All rights reserved

Table 5.2 Element compositions of slag by EDS

Element	Slag a.	Slag b.	Slag c.	Slag d.
O	45.37	32.04	33.95	35.23
Al	17.78	12.57	10.20	9.34
Si	6.73	15.66	15.39	20.74
Ca	10.12	28.81	25.96	19.25
Fe	0.00	9.06	11.81	13.20
Mg	0.00	1.86	2.68	0.00
K	0.00	0.00	0.00	2.25

Table 5.3 Chemical compositions (%w/w) of slag by XRF

Element	Slag a.	Slag b.	Slag c.	Slag d.
Na <sub>2</sub> O	0.75	0.83	0.65	1.09
MgO	2.07	3.96	3.98	2.90
Al <sub>2</sub> O <sub>3</sub>	24.79	8.78	9.80	14.41
SiO <sub>2</sub>	47.25	24.50	24.88	31.92
P <sub>2</sub> O <sub>5</sub>	0.11	0.34	0.30	0.22
SO <sub>3</sub>	0.21	0.32	0.70	0.20
K <sub>2</sub> O	3.03	0.74	1.00	1.93
TiO <sub>2</sub>	0.47	0.30	0.25	0.40
Fe <sub>2</sub> O <sub>3</sub>	11.97	20.85	20.94	17.92
MnO <sub>2</sub>	0.09	0.24	0.18	0.19
CaO	9.27	39.17	37.33	28.87

### 5.1.2 Mineral Composition

The mineral components from XRD analysis found in the slag were anorthite ( $\text{CaAl}_2\text{Si}_2\text{O}_8$ ), gehlenite ( $\text{Ca}_2\text{Al}_2\text{SiO}_7$ ), akermanite ( $\text{Ca}_2\text{MgSi}_2\text{O}_7$ ), diopside ( $\text{CaMgSi}_2\text{O}_6$ ), and esseneite ( $\text{CaFeAlSiO}_6$ ). They were related to the chemical elements, similar to previous predictions and consistent with previous reports in the literature. Anorthite was found in Slag a, the sample with the highest Si content. Gehlenite found in Slag b had the highest Ca content of the samples collected. Some of the elements found – akermanite, diopside, and esseneite – have never been reported before in the literature. Akermanite was found in Slag b and c. They were fragile. Diopside found in slag c had high hardness, in a range of 5.5-6.5 (Anthony *et al.*, 2001). Slag d was esseneite. Mg was not found in this slag. Its appearance, a fusion of lava and full of holes, differed from the others. It should be noted that XRD analysis was limited only to the crystal phases. This research was unable to determine the amorphous phases within the ash or deposits.

## 5.2 Characterization of Coal and Ash

### 5.2.1 Raw Coal Properties

The results of investigated lignite C1 and SE are shown in Appendix B. The surface morphology of both was slightly different, that the lignite SE was more irregular granules. The Ca in lignite SE was more than that in C1. The mineral composition of C1 was found to be anorthite but SE was found to be palygorskite. The hardgrove indices of lignite C1 and SE were 53 and 59, respectively.

The coals thermal characteristics were analyzed as change in weight with temperature (TG) and rate of weight loss (DTG) profiles. The degradation profiles of raw lignite samples presented at different heating rates are shown in Figures 5.1 to 5.4. Both lignite samples showed similar TG patterns with

continuous weight loss was evident. The same kinds of reactions occurred for all the heating rates considered, but the temperature ranges were different such that the TG curves shifted to higher temperatures as the heating rate increased. Three major weight loss stages can be characterized from the TG curves, corresponding to the release of moisture in the sample, the release of volatile matter and combustion of char, and the decomposition of the mineral matter in the sample (Kok et al., 2005; Sis, 2007; Sis, 2009; Chen et al., 2011). For a given heating rate, the sample A appeared to exhibit sharper changes in the TG slope than the high CaO coal, consistent with the higher negative peaks of the DTG profiles. These observations were true for the first two stages. Higher heating rate was found to show wider temperature range for mass loss. The first stage of the sample A was from 50 to about 200°C, while the first stage of the high CaO lignite covered from 50 to about 250°C. The main release of organic components and the char combustion stage for the low and high CaO lignite samples were from 200 to 575°C and 300 to 700°C, respectively. The onset of the devolatilization was delayed for the higher CaO content lignite. Thermal degradation at this second stage of mass loss showed the peak rate for the sample A to be higher than that for the sample G. From a comparison of the thermal degradation patterns, the reactions were found to take place at higher temperatures as the CaO content in the lignite increased. Since both the coal samples have similar amounts of volatile matter, they would be expected to exhibit similar thermal degradation at similar ranges of temperature (Sis, 2009). The findings implied that higher CaO containing lignite may require higher temperatures to react, but at slower rates. Table 5.4 presents the calculated values of  $E$  and  $A$  assuming the first and second order of reaction. The parameter  $A$  obtained were markedly different for the FWO and KAS, while activation energies obtained were in similar magnitude. The discrepancy between the samples A and G may be attributed to the diversity in the composition nature and the structure of the samples. The implication from the findings was that the high CaO lignite sample may be less homogeneous than the low CaO coal.

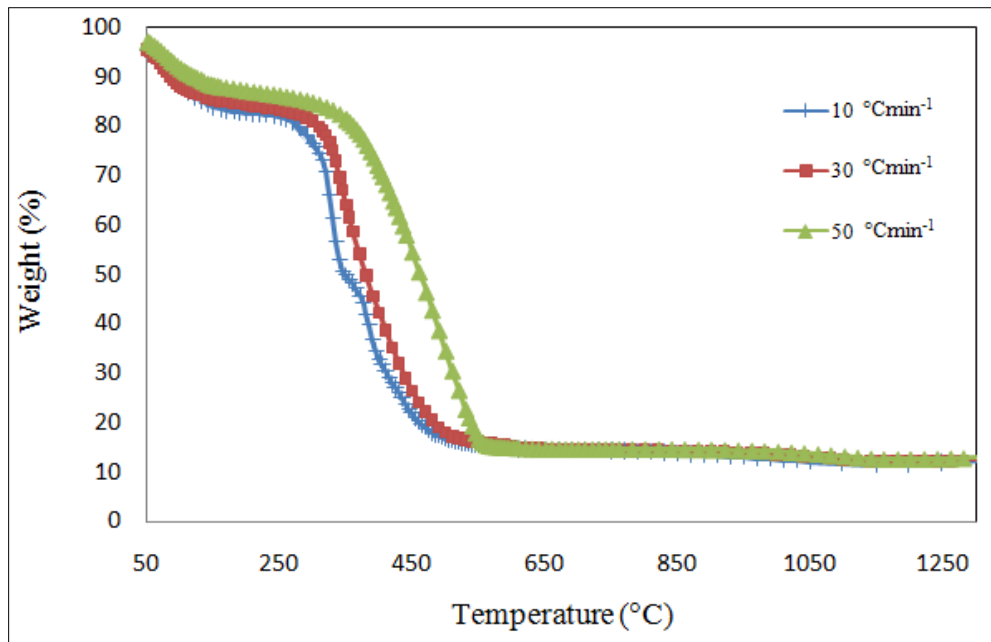


Figure 5.1 TG of sample A

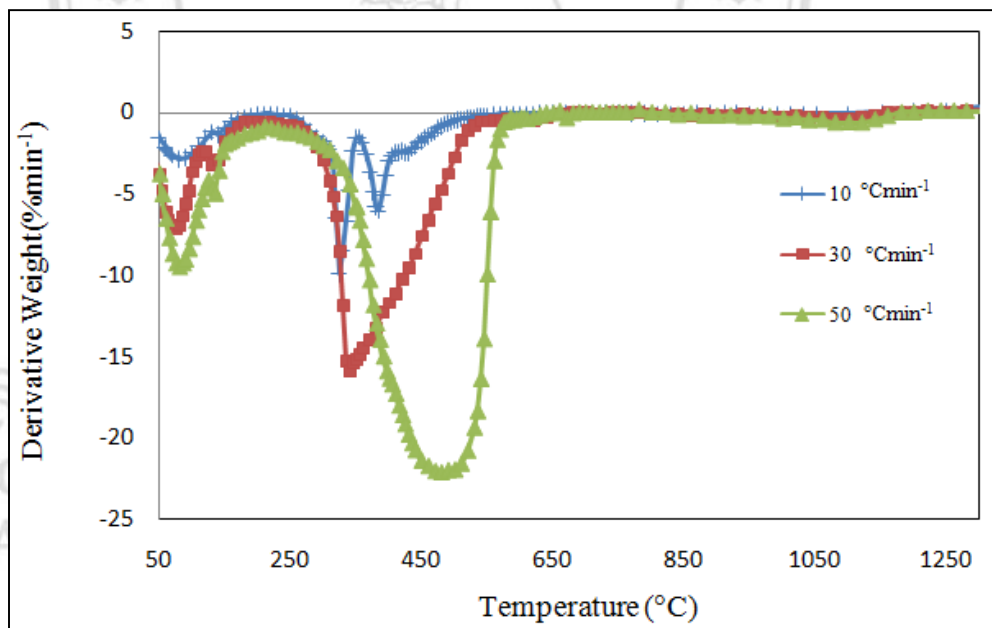


Figure 5.2 DTG of sample A

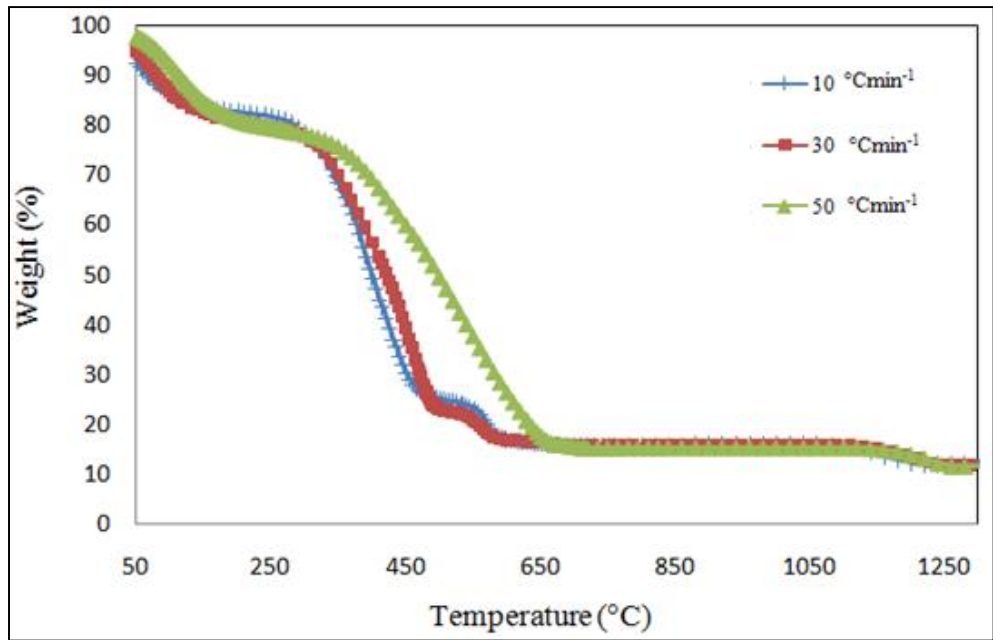


Figure 5.3 TG of sample G

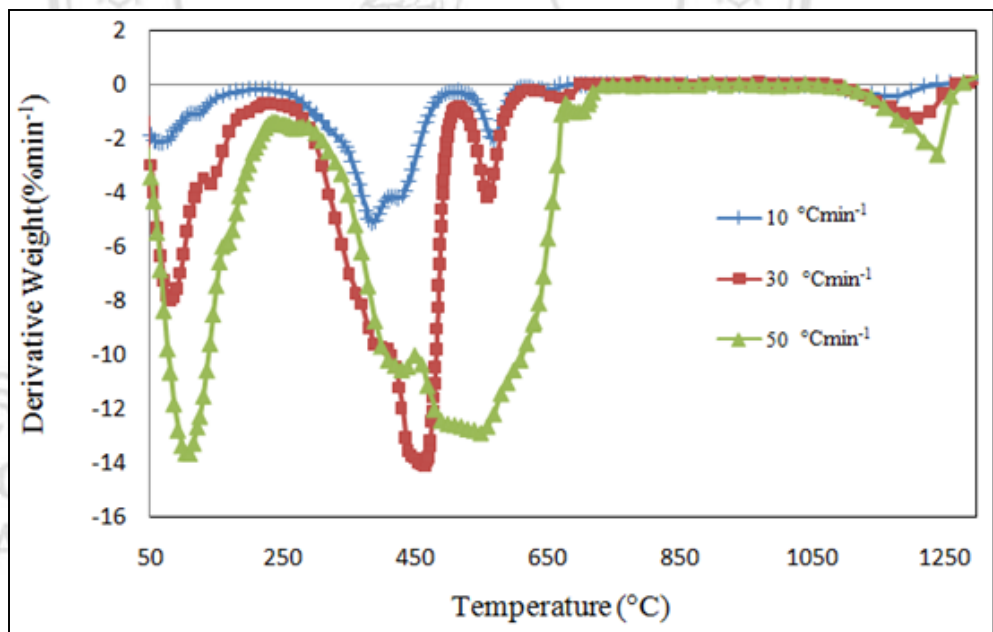


Figure 5.4 DTG of sample G



Table 5.4 Kinetic parameters of raw Mae Moh lignites

Method	Material	n	$\bar{x}$	S. D.	
FWO	Sample A	<i>E</i> (kJ/mol)	58.40	6.35	
		A	1 <sup>st</sup>	$1.30 \times 10^{-4}$	$1.04 \times 10^{-4}$
		A	2 <sup>nd</sup>	$2.13 \times 10^{-4}$	$1.64 \times 10^{-4}$
	A	3 <sup>rd</sup>	$3.89 \times 10^{-4}$	$3.08 \times 10^{-4}$	
	Sample G	<i>E</i> (kJ/mol)	88.55	46.87	
		A	1 <sup>st</sup>	$1.58 \times 10^{-5}$	$1.37 \times 10^{-5}$
		A	2 <sup>nd</sup>	$2.03 \times 10^{-5}$	$1.72 \times 10^{-5}$
		A	3 <sup>rd</sup>	$4.72 \times 10^{-5}$	$3.86 \times 10^{-5}$
		Sample A	<i>E</i> (kJ/mol)	47.25	6.30
A			1 <sup>st</sup>	$1.70 \times 10^{-2}$	$1.03 \times 10^{-2}$
A	2 <sup>nd</sup>		$2.84 \times 10^{-2}$	$1.78 \times 10^{-2}$	
Sample G	A	3 <sup>rd</sup>	$5.51 \times 10^{-2}$	$4.18 \times 10^{-2}$	
	Sample G	<i>E</i> (kJ/mol)	74.35	42.21	
		A	1 <sup>st</sup>	$1.88 \times 10^{-2}$	$2.85 \times 10^{-2}$
A		2 <sup>nd</sup>	$4.14 \times 10^{-2}$	$7.04 \times 10^{-2}$	
A	3 <sup>rd</sup>	$1.10 \times 10^{-1}$	$2.11 \times 10^{-1}$		

The other of lignite C1 and SE properties was compared and presented with blended lignites.

### 5.2.2 Chemical Properties of Blended Lignites

Proximate analysis results of blended Mae Moh lignites are shown in Table 5.5. Sample A, (the raw coal with the lowest CaO(free SO<sub>3</sub>) in ash) had the lowest moisture, but the highest in volatile matter, fixed carbon and heating value, in contrast to Sample G (the raw coal with the highest CaO(free SO<sub>3</sub>))

in ash). Samples B, C, D, E, and F were representatives of blended lignite with 20, 25, 30, 35, 40% CaO (free SO<sub>3</sub>) in ash. The results of moisture, volatile matter, ash, and fixed carbon content, were not much different, as well as the results from ultimate analysis, shown in Table 5.6. The major component of all samples was carbon. Table 5.7 presents the high and low heating values of all samples. Sample A had the highest heating value because it had the highest volatile matter and carbon content. Table 5.8 shows the ash compositions of seven lignites, with varying CaO (free SO<sub>3</sub>) in ash. The major components included Fe<sub>2</sub>O<sub>3</sub>, SiO<sub>2</sub>, SO<sub>3</sub>, Al<sub>2</sub>O<sub>3</sub>, and CaO. The minor components included Na<sub>2</sub>O, MgO, K<sub>2</sub>O, TiO<sub>2</sub>, P<sub>2</sub>O<sub>5</sub>, and MnO<sub>2</sub>. (Pipatmanomai et al., 2009).

Table 5.5 Proximate analysis (% w/w as-received basis) of blended lignite

Proximate analysis	Moisture content		Volatile matter		Ash		Fixed carbon	
	$\bar{x}$	<i>S.D.</i>	$\bar{x}$	<i>S.D.</i>	$\bar{x}$	<i>S.D.</i>	$\bar{x}$	<i>S.D.</i>
A	35.07	0.01	28.17	0.09	10.91	0.01	25.86	0.09
B	35.76	0.05	28.21	0.01	11.03	0.05	24.99	0.01
C	36.54	0.04	28.23	0.15	11.40	0.04	23.83	0.16
D	37.38	0.05	28.05	0.27	11.86	0.00	22.72	0.32
E	38.11	0.01	27.86	0.02	11.98	0.05	22.05	0.07
F	38.85	0.02	27.79	0.11	12.01	0.01	21.36	0.13
G	39.57	0.01	27.79	0.05	11.92	0.11	20.93	0.04

Table 5.6 Ultimate analysis (%w/w dry basis) of blended lignite

Ultimate analysis	Carbon		Hydrogen		Nitrogen		Oxygen		Sulfur	
	$\bar{x}$	<i>S.D.</i>	$\bar{x}$	<i>S.D.</i>	$\bar{x}$	<i>S.D.</i>	$\bar{x}$	<i>S.D.</i>	$\bar{x}$	<i>S.D.</i>
A	58.54	0.01	3.00	0.00	1.89	0.00	12.88	0.03	5.49	0.03
B	58.49	0.04	2.95	0.01	1.86	0.00	12.77	0.01	5.35	0.01
C	58.49	0.04	2.95	0.01	1.86	0.00	12.77	0.01	5.35	0.01
D	58.43	0.04	2.72	0.01	1.86	0.00	11.80	0.10	4.76	0.03
E	58.41	0.01	2.63	0.00	1.86	0.00	11.90	0.05	4.29	0.01
F	58.39	0.08	2.55	0.00	1.84	0.00	12.01	0.01	3.94	0.04
G	58.35	0.01	2.44	0.00	1.81	0.00	12.63	0.15	3.33	0.01

Table 5.7 Heating value (MJ/kg dry basis) of blended lignite

Heating Value	HHV		LHV	
	$\bar{x}$	<i>S.D.</i>	$\bar{x}$	<i>S.D.</i>
A	22.80	0.07	22.15	0.07
B	22.76	0.00	22.12	0.00
C	22.58	0.02	21.97	0.02
D	22.44	0.00	21.86	0.00
E	22.38	0.01	21.81	0.01
F	22.27	0.02	21.73	0.02
G	22.08	0.01	21.55	0.01

Table 5.8 Ash composition (% mass) of blended lignite

Compositions		A	B	C	D	E	F	G
SiO <sub>2</sub>	$\bar{x}$	21.28	19.51	19.60	18.14	19.24	17.45	17.22
	<i>S.D.</i>	0.19	0.01	0.49	0.48	1.37	1.47	0.93
Al <sub>2</sub> O <sub>3</sub>	$\bar{x}$	13.43	9.89	7.39	5.00	3.38	1.54	1.31
	<i>S.D.</i>	0.00	0.06	0.15	0.01	0.17	0.04	0.18
TiO <sub>2</sub>	$\bar{x}$	0.24	0.18	0.15	0.10	0.08	0.05	0.05
	<i>S.D.</i>	0.01	0.01	0.01	0.00	0.01	0.00	0.00
CaO	$\bar{x}$	11.08	14.71	19.07	21.02	25.12	27.68	27.96
	<i>S.D.</i>	0.44	0.14	0.66	0.06	1.55	0.60	0.27
Fe <sub>2</sub> O <sub>3</sub>	$\bar{x}$	28.03	24.83	22.93	20.03	19.10	16.19	15.98
	<i>S.D.</i>	1.19	0.27	0.72	0.17	1.08	0.53	0.08
Na <sub>2</sub> O	$\bar{x}$	1.87	1.47	1.30	1.04	0.81	0.67	0.74
	<i>S.D.</i>	0.10	0.06	0.00	0.04	0.08	0.02	0.08
MgO	$\bar{x}$	4.02	3.57	3.45	3.22	3.24	3.24	3.46
	<i>S.D.</i>	0.23	0.10	0.17	0.03	0.09	0.07	0.08
K <sub>2</sub> O	$\bar{x}$	1.31	0.96	0.71	0.48	0.32	0.16	0.15
	<i>S.D.</i>	0.02	0.03	0.03	0.00	0.03	0.00	0.01
SO <sub>3</sub>	$\bar{x}$	18.64	24.73	25.22	30.71	28.47	32.73	32.86
	<i>S.D.</i>	1.73	0.15	2.22	0.63	4.41	2.53	0.71
P <sub>2</sub> O <sub>5</sub>	$\bar{x}$	0.07	0.11	0.14	0.17	0.20	0.22	0.22
	<i>S.D.</i>	0.00	0.02	0.00	0.00	0.02	0.01	0.01
MnO <sub>2</sub>	$\bar{x}$	0.04	0.05	0.05	0.06	0.07	0.07	0.07
	<i>S.D.</i>	0.00	0.00	0.01	0.00	0.01	0.00	0.00
CaO	$\bar{x}$	13.62	19.54	25.50	30.34	35.12	41.15	41.64
freeSO <sub>3</sub>	<i>S.D.</i>	0.25	0.16	0.12	0.19	0.01	0.65	0.85

### 5.2.3 Thermal Properties of Blended Lignite

For thermal properties of blended lignite ash, ash fusibility temperatures are shown in Table 5.9. The scattering in the data was found to be small, less than 7% of the corresponding average value. It should be noted that the ash at the tip of the cone in the AFT test can have slight variations from the overall composition, which may affect the measured AFT (Seggiani, 1999). The results were consistent with Luxanayothin et al. (2010), which showed that the high CaO in ash affected low ash fusion temperatures. Figure 5.5 presents the ash fusion temperatures at different CaO(free SO<sub>3</sub>) in ash. The lignite E (35.11% of CaO (freeSO<sub>3</sub>) in coal ash) was found to have the lowest ash melting point and IT-FT gap, thus indicating highest potential to a severe slagging problem. This may be contributed to its conclusion that the other elements in the ash affected the AFT.

Table 5.9 Ash fusibility temperatures (°C) results of blended lignite

Ash fusibility temperatures	IT		ST		HT		FT	
	$\bar{x}$	<i>S.D.</i>	$\bar{x}$	<i>S.D.</i>	$\bar{x}$	<i>S.D.</i>	$\bar{x}$	<i>S.D.</i>
A	1235	69	1305	10	1340	14	1480	5
B	1205	7	1270	3	1280	4	1475	4
C	1205	18	1230	13	1235	15	1250	20
D	1205	3	1220	4	1225	7	1240	10
E	1205	6	1215	2	1220	3	1225	3
F	1210	80	1260	3	1260	3	1280	8
G	1235	31	1260	14	1265	18	1300	21

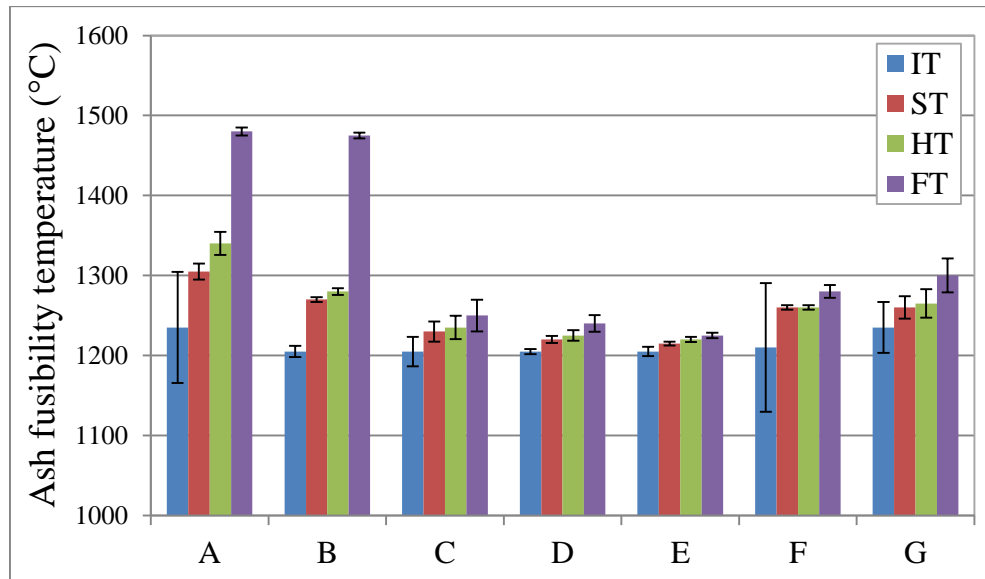


Figure 5.5 Relationship between the ash fusion temperatures with % of CaO (free SO<sub>3</sub>) in the ash of all the samples

### 5.3 Effect of Ca in Ash on Slag Formation and Deposition

The oxide compositions in the ash samples were used to calculate the parameter of slag formation and deposition. The results are shown in Table 5.9. It was found that the base/acid ratio of sample A was the lowest value at 1.33. It was greater than 1.0, indicating high potential of slag. Samples B, C, D, E, F, and G were higher than sample A, respectively, which would probably be higher than the slag potential as well. However, only one parameter could not clearly indicate the potential. The silica/alumina ratio of sample E, F, and G was higher than general range (0.8 to 4.0), making the sample to have lower ash fusion temperatures. At the same values at lower 1.7, the ash fusion temperatures were markedly increased from sample A (Singer, 1981). The iron/calcium ratio was greater than 3:2 in samples E, F, and G. The results affected higher fluxing of ash. This was consistent with the results of fused ash characterization in Table 5.6. The iron/dolomite ratio was less than one in samples D, E, F, and G. This probably indicated that there were more fluxing properties in these samples.

Table 5.10 Results of blended lignite to slag formation and deposition parameters

Parameters	B/A	Silica/Alumina	Iron/Calcium	Iron/Dolomite
A	1.33	1.58	2.53	1.86
B	1.54	1.97	1.69	1.36
C	1.75	2.66	1.20	1.02
D	1.97	3.62	0.95	0.83
E	2.14	5.69	0.76	0.67
F	2.52	11.29	0.59	0.52
G	2.60	13.14	0.57	0.51

Table 5.11 shows different appearances of the fused ash samples. The characterization of fused ash A and B like the porous media, that seem to be eliminated cheaply. Fused ash C, D, E, F, and G, were dense in the refractory substrate. Especially, the fused ash F, and G, were melted flux. These results were consistent with the results from the iron/calcium ratio ratio and the iron/dolomite ratio. The SEM results encouraged the different morphologies of ash fused. The fused ash of samples A and B morphologies surface were similar to the real slag. The samples C and D were slightly different, showing the sphere on the upper surface. The sphere probably was the calcium aluminate ( $\text{CaAl}_2\text{O}_4$ ) because the EDS results observed the calcium and aluminum content (Fernandez-Turiel et al., 2004). The fused ash of sample E and F, shows the crystallized phase with stubby calcium ferrite crystals (Huggins et al., 1981). Fused ash of sample G is different. It can be seen that it melted like homogeneous. These results indicated that slag from sample E (the lowest ash fusibility temperatures) was the easiest formation of slag in boiler furnace, and difficult to remove.

Table 5.11 Characterization and surface morphology feature of the fused ash


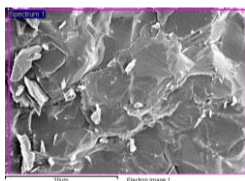

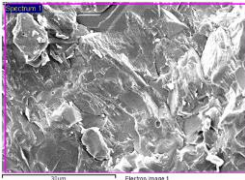

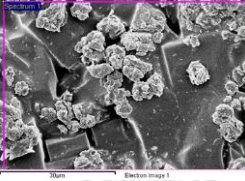

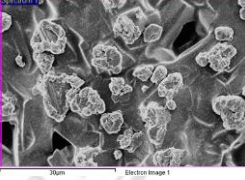

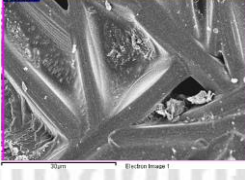

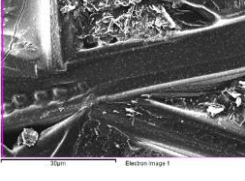

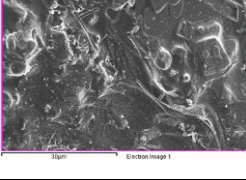
Sample	Characterization	Surface morphology
A		
B		
C		
D		
E		
F		
G		



Table 5.12 Element compositions of the fused ash by EDS

Element	O	C	Mg	Al	Si	Ca	Fe
A	14.76	0.00	0.00	16.02	8.38	4.81	56.03
B	34.32	13.39	0.00	32.08	12.41	7.80	0.00
C	19.98	15.60	3.38	6.66	11.94	13.26	29.17
D	26.50	7.62	2.59	4.64	11.10	14.42	33.14
E	42.94	6.82	1.95	3.85	17.62	26.82	0.00
F	37.55	5.29	1.59	3.27	13.42	25.00	13.89
G	33.66	6.97	0.00	36.28	10.73	12.36	0.00

## 5.4 Slag Formation Prediction

### 5.4.1 Equilib Model

The mineral transformation and slag-liquid formation of blended lignites are predicted by Equilib model. As the temperature increases to 950°C, the slag-liquid starts to form. The solids at a temperature of 800 °C such as hematite ( $\text{Fe}_2\text{O}_3$ ), anhydrite ( $\text{CaSO}_4$ ), Anorthite ( $\text{CaAl}_2\text{Si}_2\text{O}_8$ ) and high-albite ( $\text{NaAlSi}_3\text{O}_8$ ), decrease at higher temperatures. The details of Equilib model are shown in Appendix B. The slag-liquid increases at the higher temperatures. The relationship between the temperature and the mass percent of liquid phase of slag of the samples is shown in Figure 5.6, referring to the slag-liquid types 1 and 2. Figure 5.7 presents the total of slag-liquid. The results observed indicate that the slag-liquid form of the samples C, D, and E have higher slagging potential. This can be used in the design temperature in the boiler furnace.

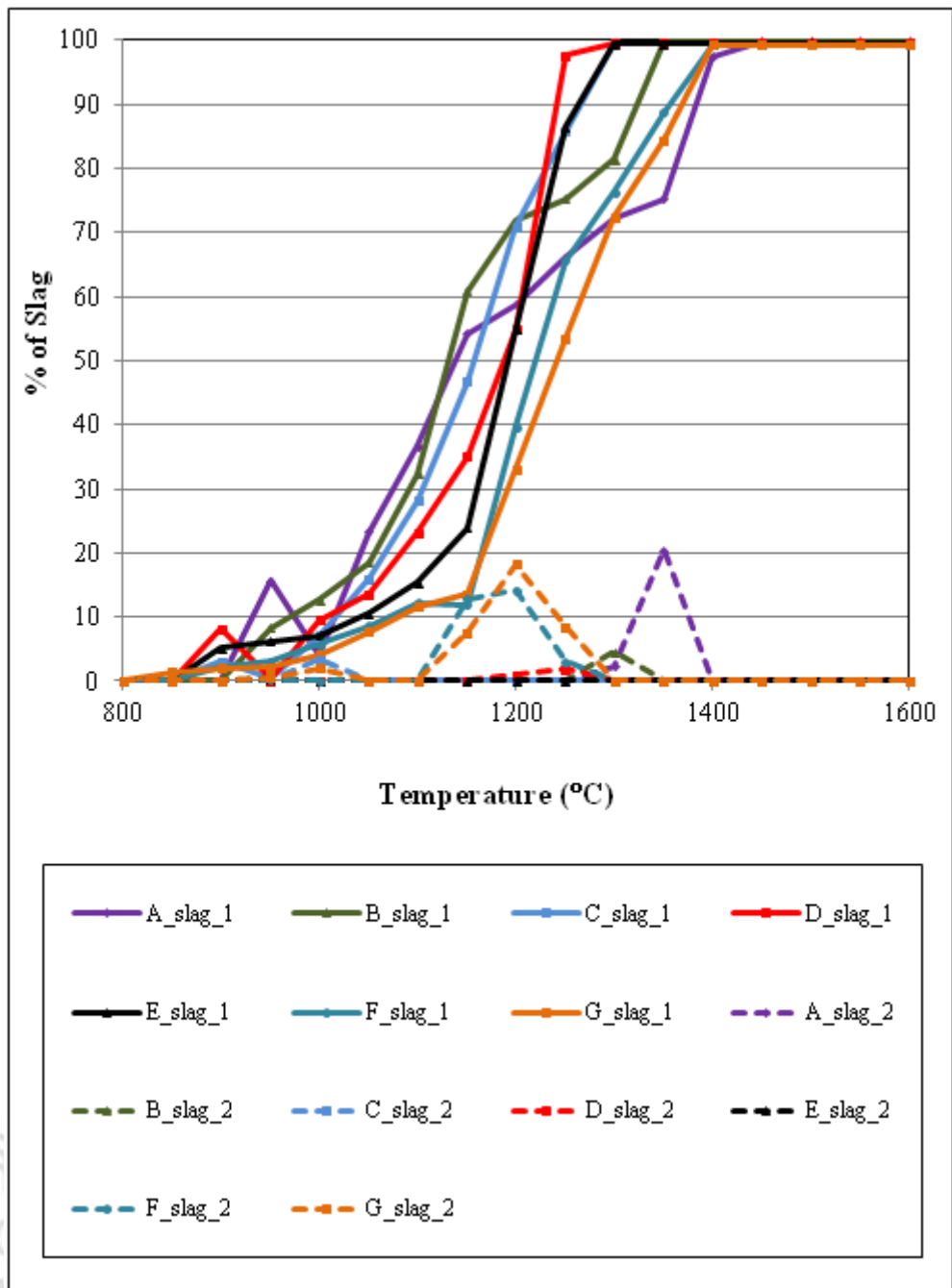


Figure 5.6 Percent of slag types 1 and 2 from prediction at different temperature

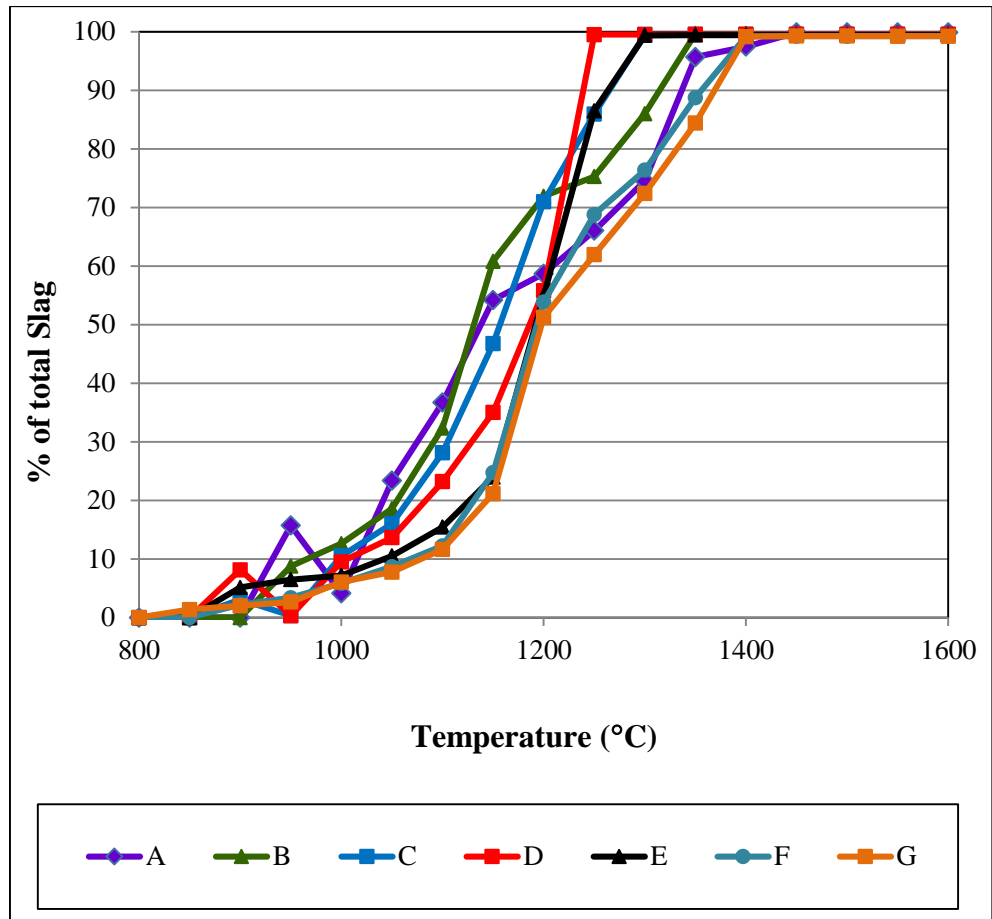


Figure 5.7 Percent of total slag from prediction at different temperature

The slag compositions are shown in Table 5.13. The main compositions of slag\_1 were CaO, Fe<sub>2</sub>O<sub>3</sub>, and SiO<sub>2</sub>, whilst, Fe<sub>2</sub>O<sub>3</sub> was just only in the main composition in slag\_2. However, this study focuses on the slag liquid form, which includes 2 types of the predicted slag potential. The Equilib model can predict the quantity and identify the details.

Table 5.13 Oxide compositions in predicted slag-liquid

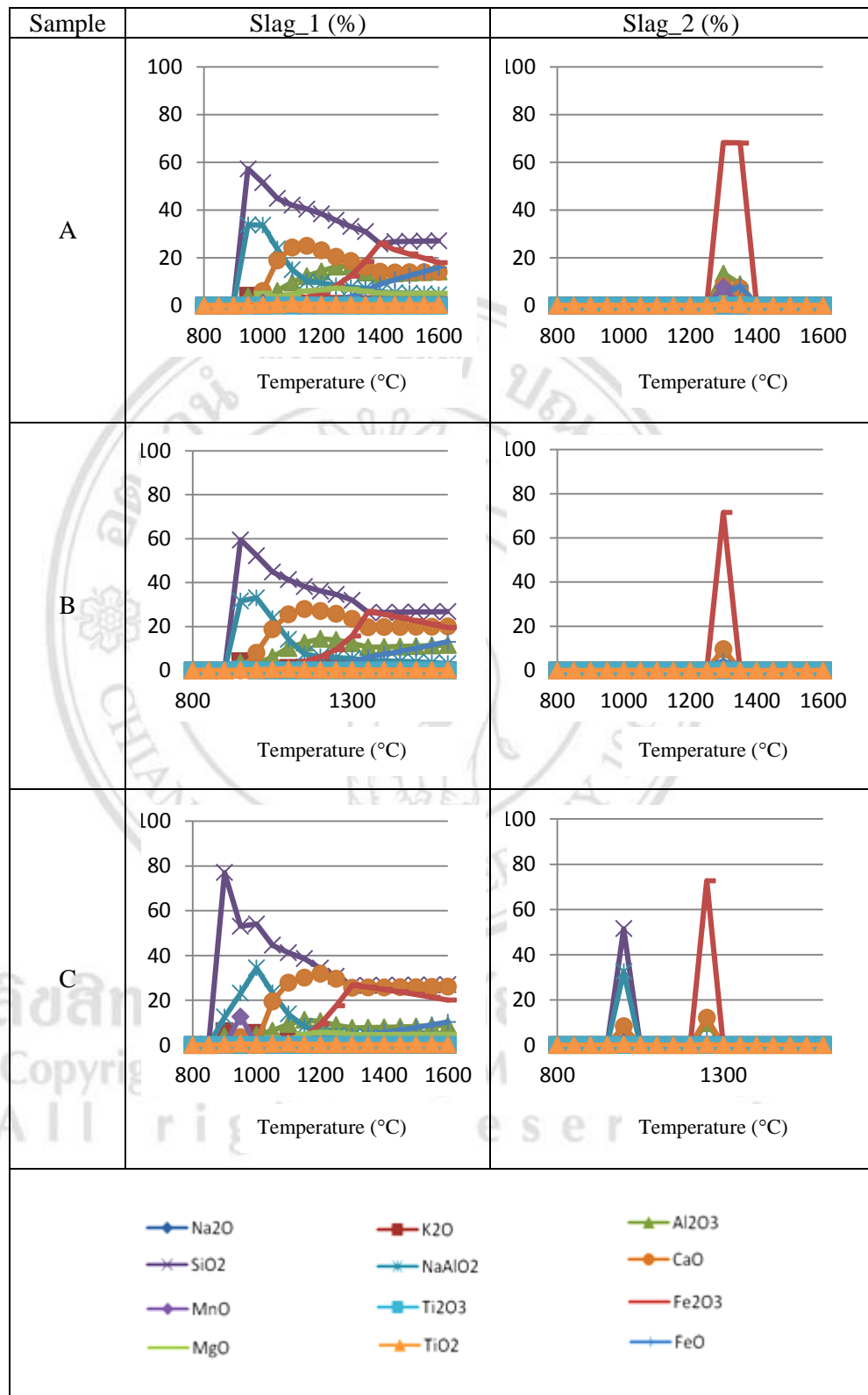


Table 5.13 (continue)

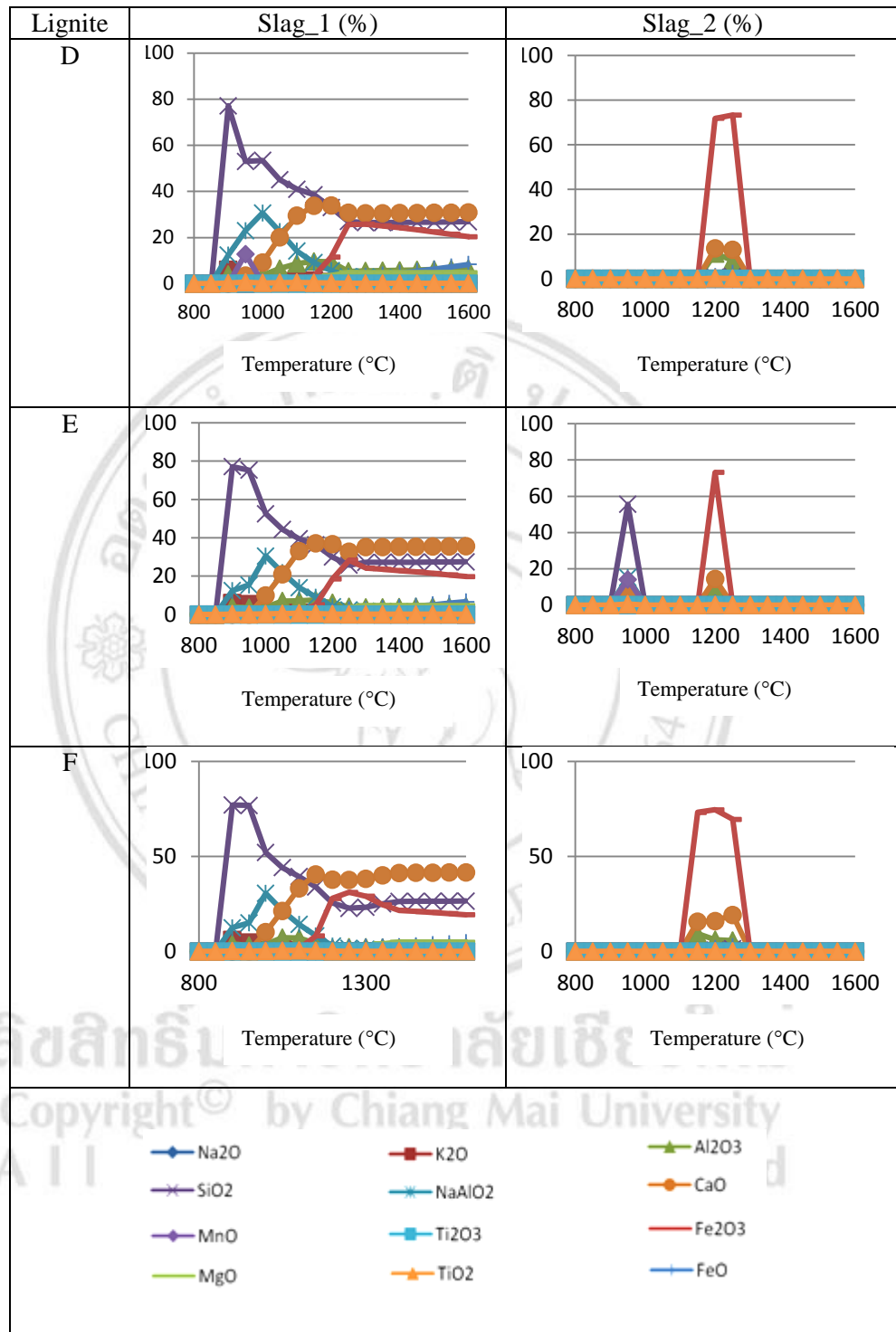
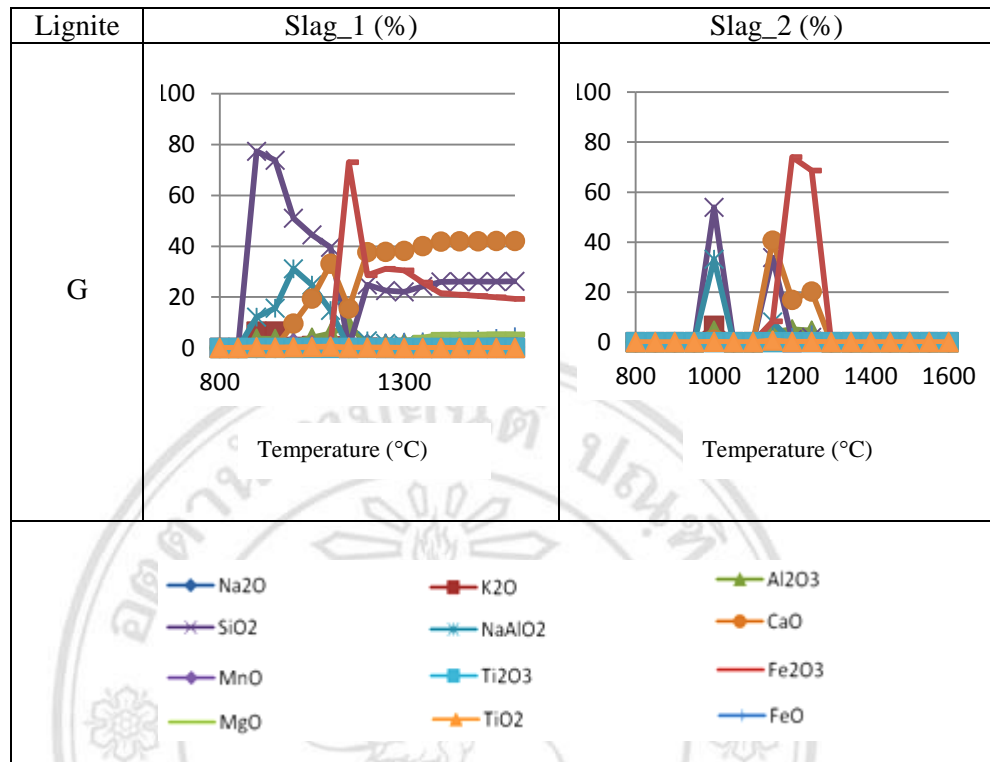


Table 5.13 (continue)



#### 5.4.2 Phase Diagram Model

In the simulation, the calculation can be extremely slow if all ash compositions are input into the module. Therefore, in this work, only the main compositions ( $\text{SiO}_2$ ,  $\text{Al}_2\text{O}_3$ ,  $\text{CaO}$ , and  $\text{Fe}_2\text{O}_3$ ) in ash of blended coal were selected to plot against fusion temperature in ternary phase diagram. First, the ternary phase diagram was calculated with the ash components on the control condition. The  $\text{SiO}_2$ - $\text{Al}_2\text{O}_3$ - $\text{CaO}$  system is shown in Fig. 5.8. By increasing the  $\text{CaO}$  content up to 25.50%, the liquidus temperature decreased from  $1500^\circ\text{C}$  reaching the lowest value at  $1300^\circ\text{C}$ , but increased upto  $1600^\circ\text{C}$  area. Similar patterns for the melting temperature were also observed with decreasing contents of acidic ( $\text{SiO}_2$  and  $\text{Al}_2\text{O}_3$ ) components. This predicted trend was similar to the measured AFT between 13.62-25.50 % $\text{CaO}$  (free  $\text{SO}_3$ ) content but a marked difference was observed between prediction and measurement for the % $\text{CaO}$  (free  $\text{SO}_3$ ) content from 30.34-41.64. From the present phase diagram, the lignite C was the lowest fusion temperature, in consistent with the AFT measurement. This implies that the

SiO<sub>2</sub>-Al<sub>2</sub>O<sub>3</sub>-CaO system was not one of the critical phase formations affecting the AFT in the blended coal. This may be contributed to the fact that elements other than CaO may have stronger influence on AFT. However, these three oxides were still being used in the simulation, because of the combined oxides of up to 50% in ash.

The mineral of slag were found in the results of phase diagram. The minerals were anorthite (CaAl<sub>2</sub>Si<sub>2</sub>O<sub>8</sub>), wollastonite (CaSiO<sub>3</sub>), rankinite (Ca<sub>3</sub>Si<sub>2</sub>O<sub>7</sub>), and calcium silicate (Ca<sub>2</sub>SiO<sub>4</sub>).

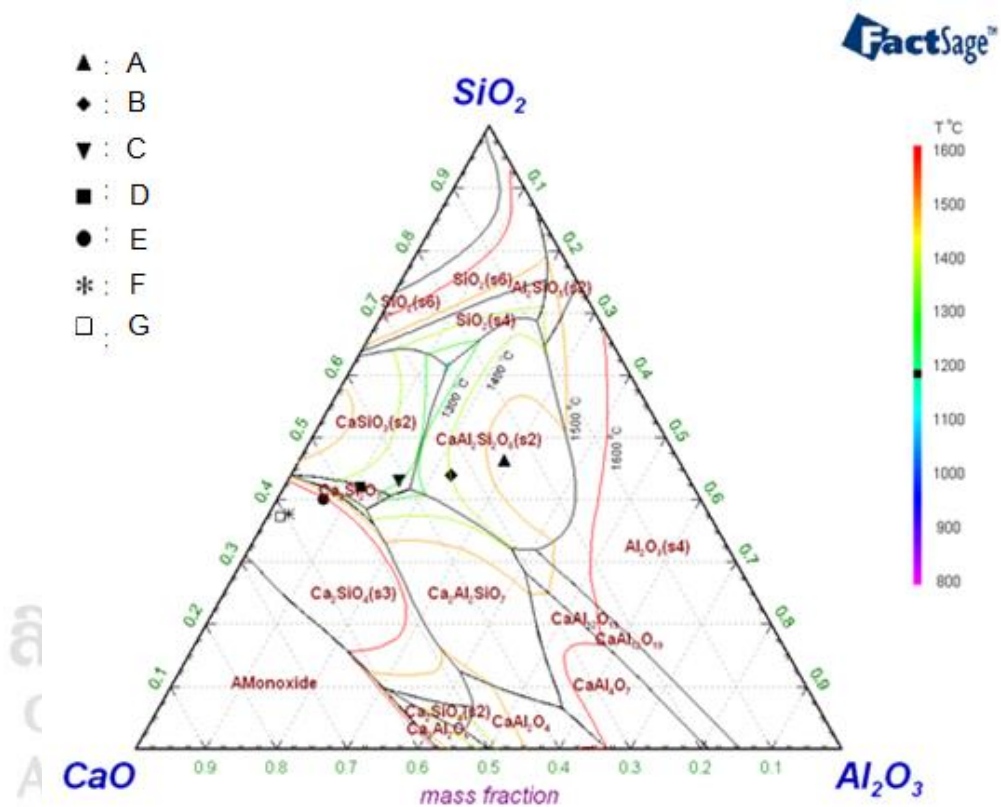


Figure 5.8 Mineral phase diagram and liquidus surface of SiO<sub>2</sub>-Al<sub>2</sub>O<sub>3</sub>-CaO system

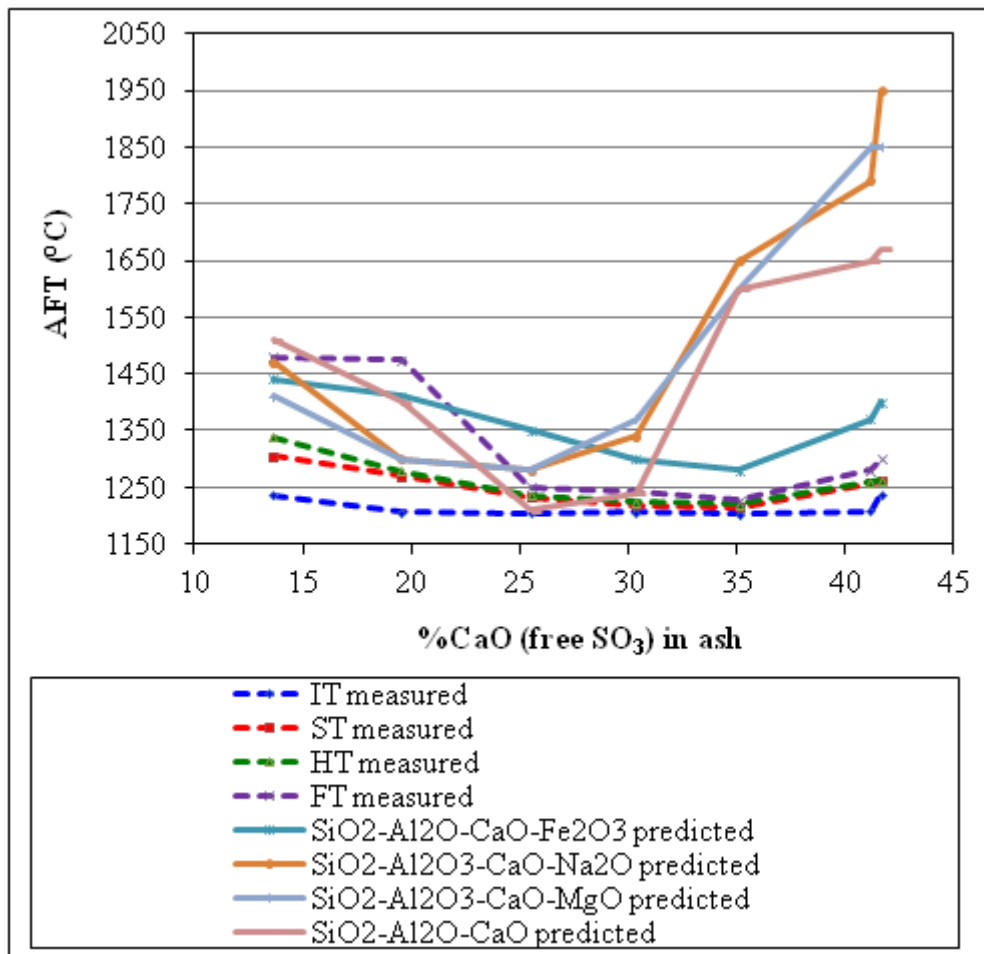


Fig. 5.9 Measured (dotted lines) and predicted (solid lines) ash fusion temperatures with different CaO (free SO<sub>3</sub>) content in the ash

The quaternary diagram was used to predict liquidus temperatures of ash. Because of four compositions calculation, long computation was required. Due to the fact that superimpose function in FactSage was used in quaternary diagram, the phase of mineral can not be predicted. Only the liquidus temperatures were predicted. It was therefore necessary to consider the phase diagram with four components. Three quaternary diagrams with varying temperatures were used to predict the ash fusion temperature of SiO<sub>2</sub>-Al<sub>2</sub>O<sub>3</sub>-CaO with Fe<sub>2</sub>O<sub>3</sub>, SiO<sub>2</sub>-Al<sub>2</sub>O<sub>3</sub>-CaO with Na<sub>2</sub>O, and SiO<sub>2</sub>-Al<sub>2</sub>O<sub>3</sub>-CaO with MgO systems.



The simulated results are shown in Fig. 5.9, along with the AFT from the measurement. They were found to exhibit a non-linear behavior with respect to the ash compositions. The effect of CaO in the ash on AFT was apparent. Unlike Na<sub>2</sub>O and MgO, the quaternary system with additional Fe<sub>2</sub>O<sub>3</sub> was found to be qualitatively and quantitatively similar to the measurement. The Fe<sub>2</sub>O<sub>3</sub> appeared to be one of the major compositions affected by the ash fusion temperature. According to previous research on the SiO<sub>2</sub>-Al<sub>2</sub>O<sub>3</sub>-CaO-Fe<sub>2</sub>O<sub>3</sub> system, the lowest AFT was observed at 35% of the CaO content disregard of the SO<sub>3</sub> content (Song et al., 2010). Using the FactSage program, the time and cost of testing AFT can be reduced.

From the findings, lignite E (35.12%CaO (free SO<sub>3</sub>), 19.24% SiO<sub>2</sub>, 3.38% Al<sub>2</sub>O<sub>3</sub>, 25.12% CaO, and 19.10% Fe<sub>2</sub>O<sub>3</sub>) showed low fusion temperature, and may pose a severe slag problem when the boiler furnace temperature is above 1300°C. The possible reason for this behavior is that the the oxide of Ca, Fe, Si, and Al may have an interaction effect that significantly influences the slagging potential.

### **5.5 Slag Deposition Prediction**

The initial simulation was run and convergence was ensured for grid independent test. The results of grid solution value that was independent are shown in Figures 5.10 and 5.11. The velocity of interested areas at 308,940 computer grid cells shows nearly constant value as the temperature. The results may have large variation because the shape of the grid is different after changing the grid numbers. The geometry with 308,940 computer grid cells was chosen to predict the deposition of slag in FLUENT.

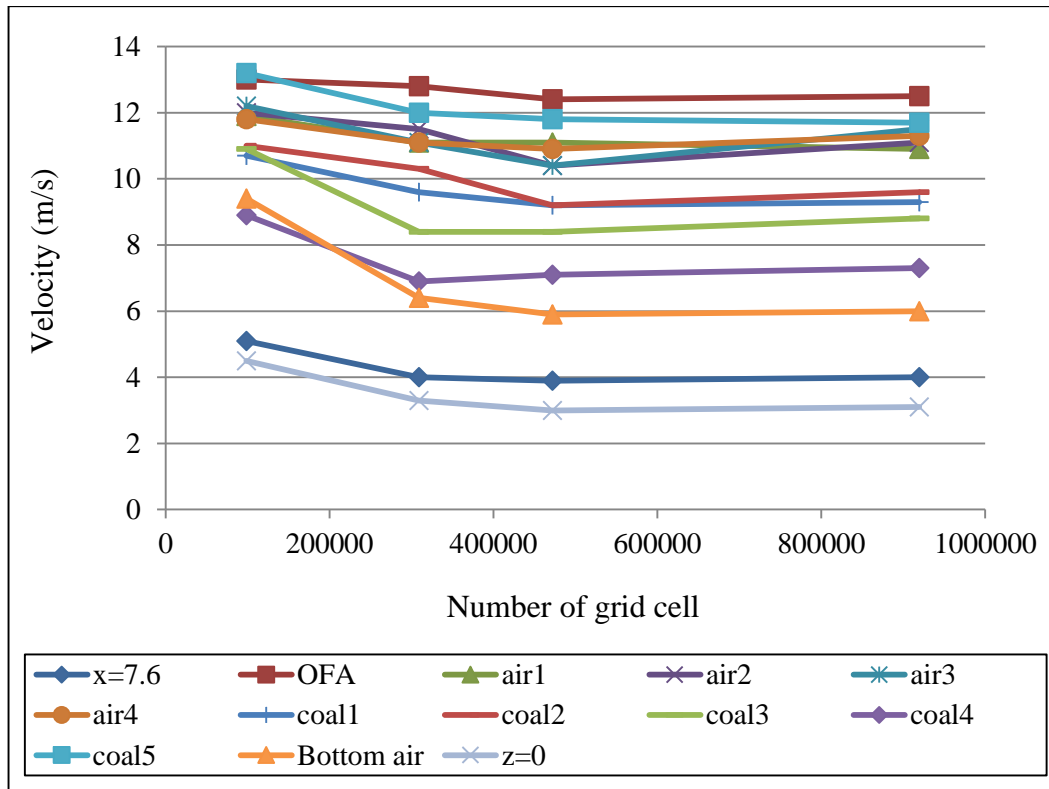


Figure 5.10 The convergence results of velocity at the panels

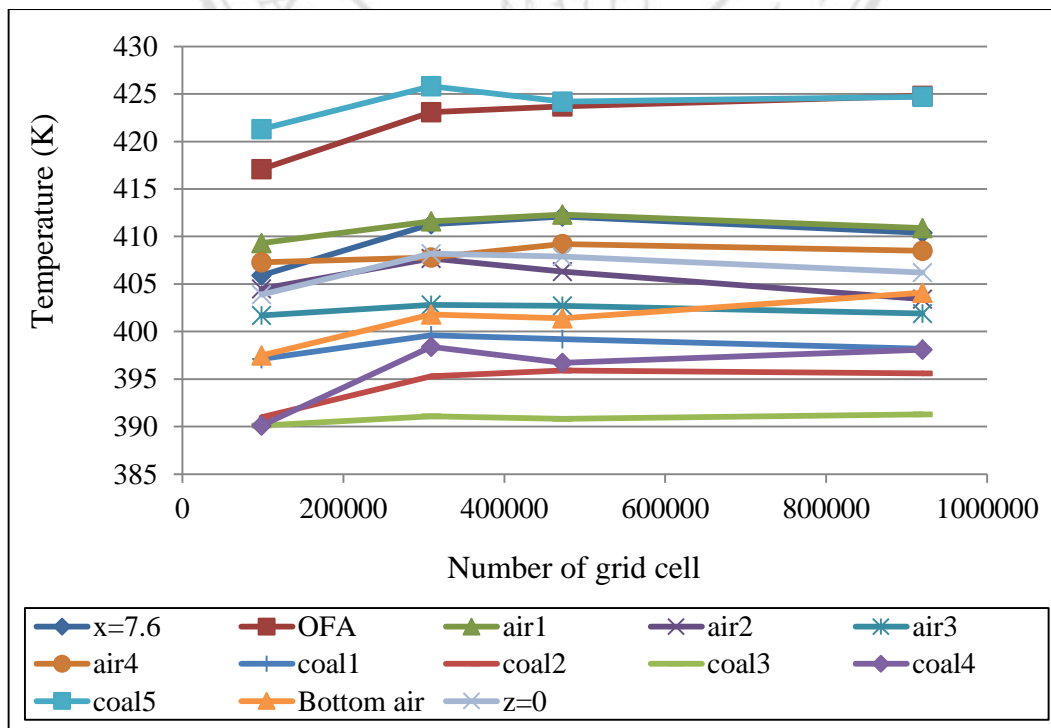


Figure 5.11 The convergence results of temperature at panels

The temperature inside the boiler is shown in Figure 5.12. The direction of the fireball likes the swirling flow. The high temperature of gas was found near the burner zone and the temperature was reduced at the superheater and reheater zones. The flue gas temperature at the exit furnace was about 1600°C, higher than the measured value (Appendix D) because the temperature for patch region for ignition was 1700°C. Figure 5.13 shows the fluid temperature at the boiler wall. Figure 5.14 shows the temperature regions, are close to the inlets. The temperatures at the secondary air, and over fire air inlet, are higher than at pulverized coal, and bottom air inlet because that are stoichiometric combustion areas. The fluid temperature on right side of the burner showed a lower temperature. Because the swirl counterclockwise, the temperature of coal and air inlet are lower after combustion. The temperature can be used to predict the deposition of slag, using with the fusion temperature of the ash. If the temperature higher than the ash fusion temperature, it is likely to cause the slag to stick to the wall and affect to higher deposition of slag. It can be seen that if the slag that stick to the walls of furnace to the mechanism of slag solidification, because the temperature of the wall (Figure 5.15) is lower than the temperature of the slag.

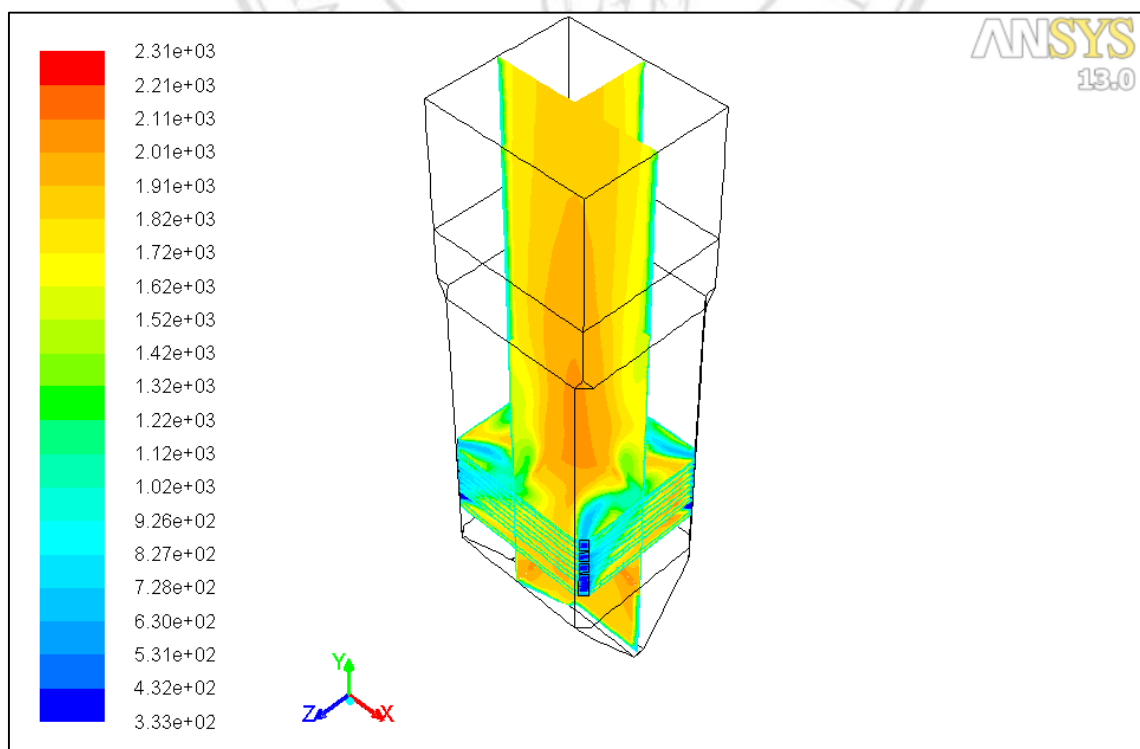


Figure 5.12 Temperature distribution isosurface of coal combustion in boiler

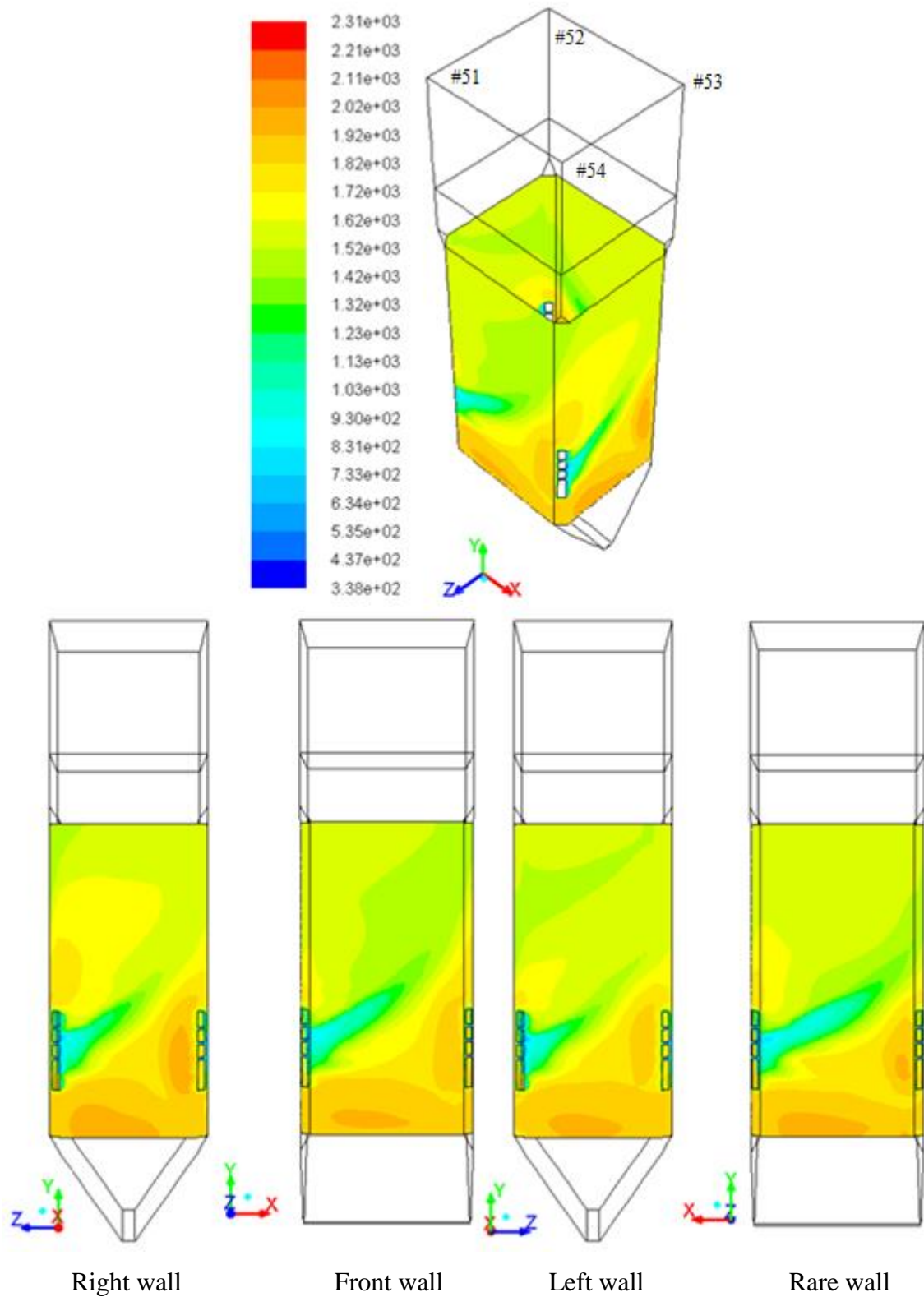


Figure 5.13 Temperature at the boiler wall

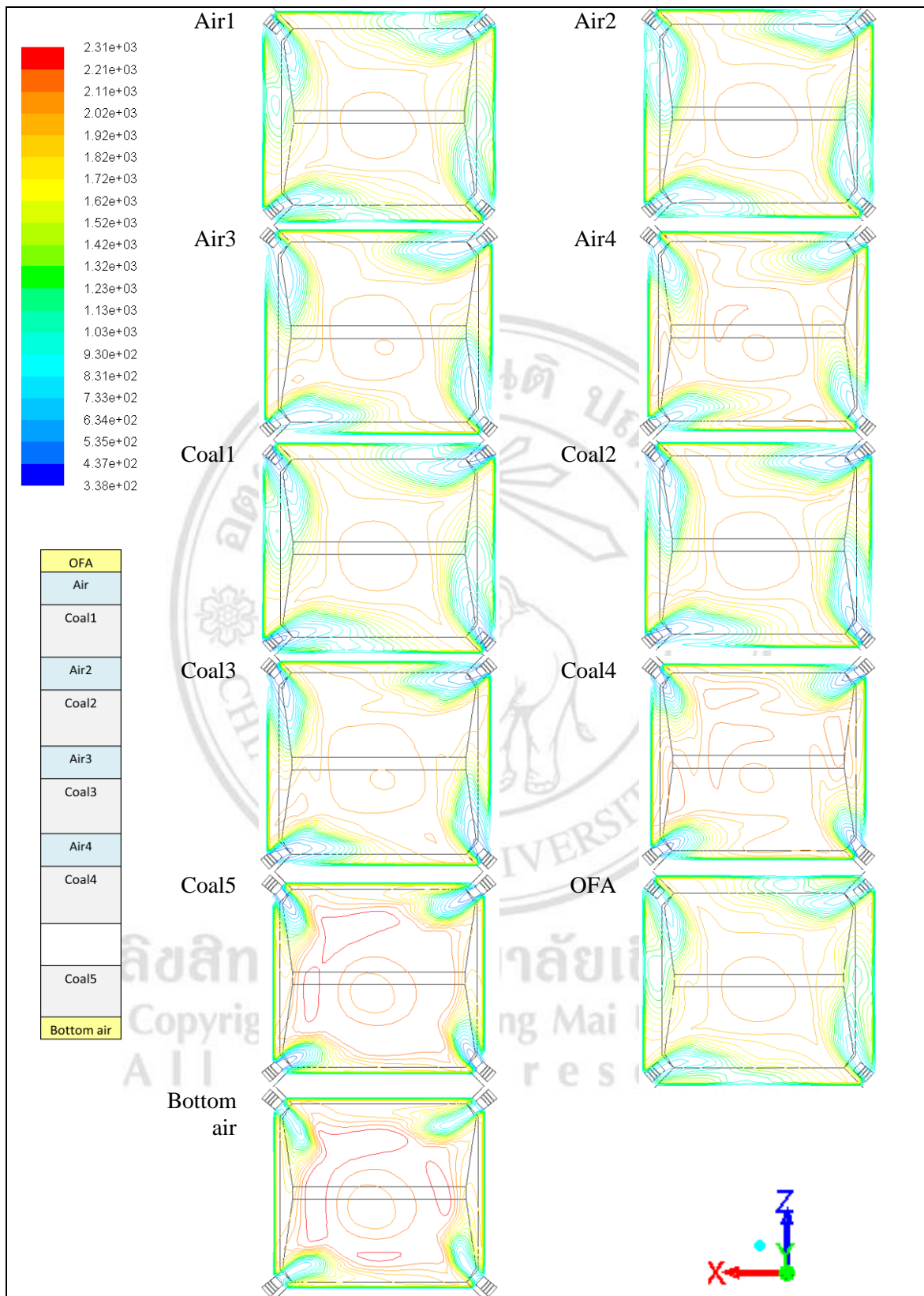


Figure 5.14 Temperature contours of coal combustion in boiler at the inlet panel

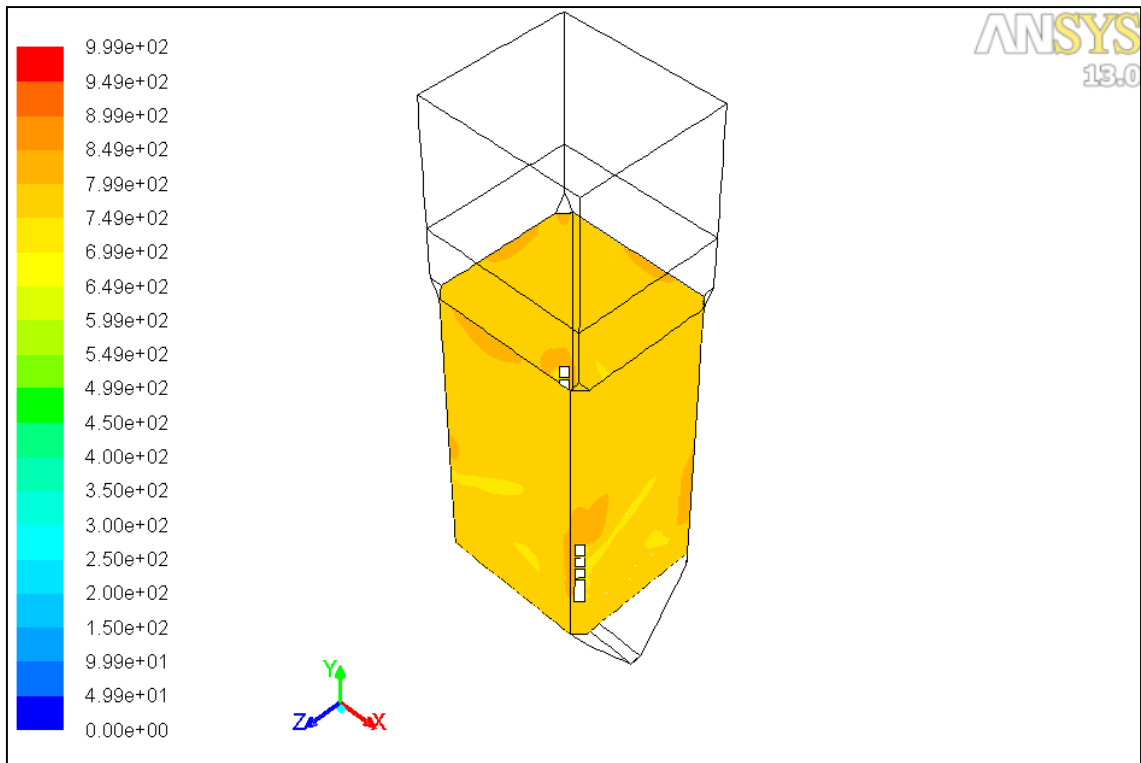


Figure 5.15 Temperature of the boiler wall

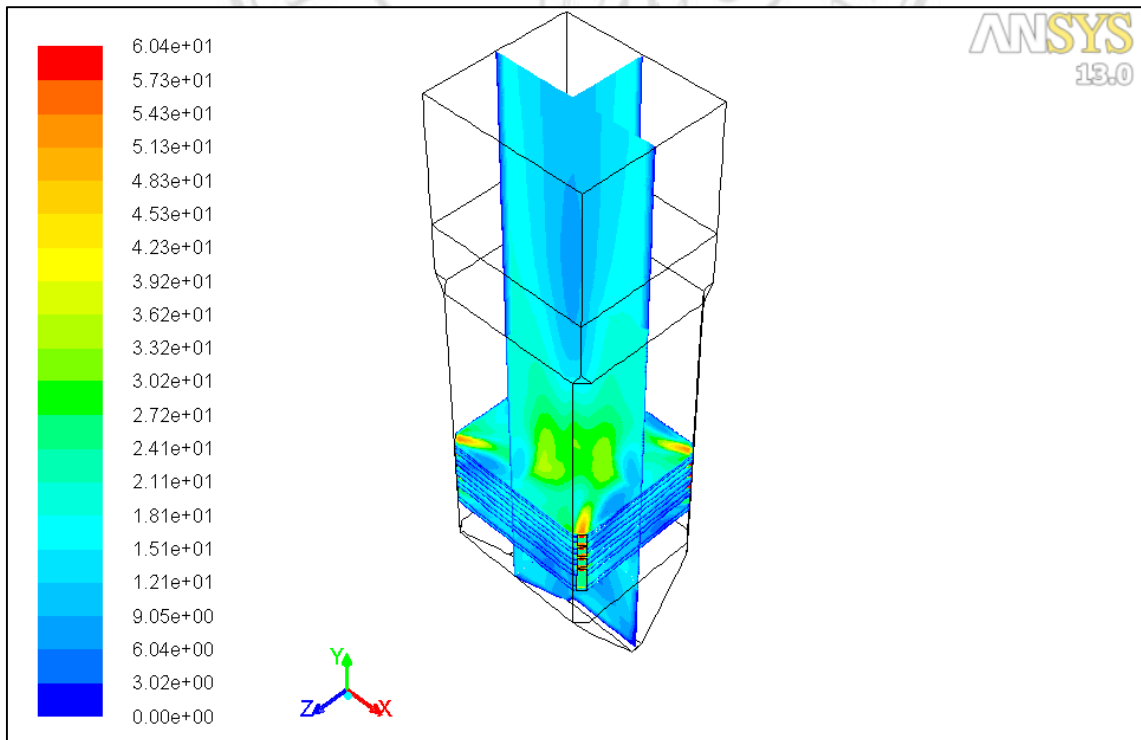


Figure 5.16 Velocity distribution isosurface of coal combustion in boiler

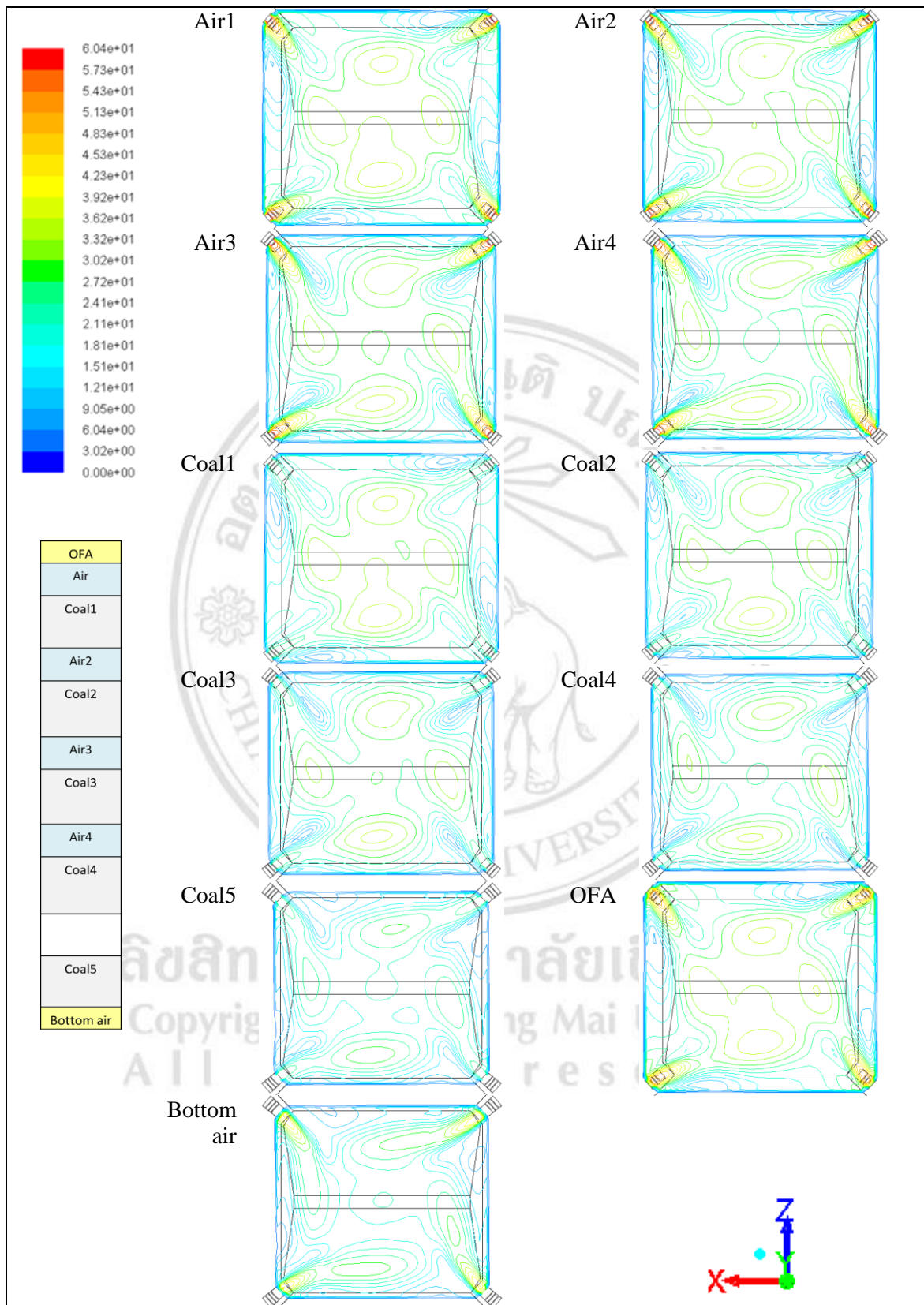


Figure 5.17 Velocity contours of coal combustion in boiler at the inlet panel

However, also consider other factors such as the flow velocity in the boiler furnace. The velocity distributions are showed in the Figure 5.16 and 5.17. The area has a low velocity, which causes the deposition of dead spots easily. That is the right side of the burner. The flow field, and the particle trajectory are shown in Figures 5.18 and 5.19 respectively. The fire ball rotation is counter clockwise: from corner#51 to corner#54, corner#53, and corner#52. The particles are in the same direction. Then the particles are inside the boiler, the temperature was higher with combustion reaction. Some particles were tracked with the wall, that probably sticking on the furnace wall if the wall temperature is higher than ash fusion temperature.

The locations of surface heat flux sensors are shown in Figure 5.20. Generally, the 28 sensors were operated and the data was collected by FACOS system. Figure 5.21 presents the surface heat flux form case study simulation. The results were compared against the measured heat flux of the Mae Moh boiler. Qualitatively, the predicted heat flux in the region of the heat flux sensors were in agreement with the measure data, Figure 5.22. The coal properties were different, that affected the assessing of slag deposition. The lignite SE from the Mae Moh mine with high CaO content may have high slagging potential. The discrepancies between the predicted and measured data were believed to be mainly due to the boundary conditions used in the CFD model (Garba, 2012), because some of boundary conditions were difficult to determine correctly for the boiler in real operation. Besides some of the real coal properties data were missing. The reference values were used instead. The location of the sensors was not given in x and y directions. The data of measuring heat flux was of average value. They could affect the accuracy of the prediction.

However, the results seemed to be good prediction because the predicted heat flux showed similar trend with the real data. The predicted results were compared with the deposition of slag in the actual operation of Mae Moh power plant, as shown in Figure 5.23. It can be seen that the deposition zone as consistent, which is the burner zone with especially in right side.



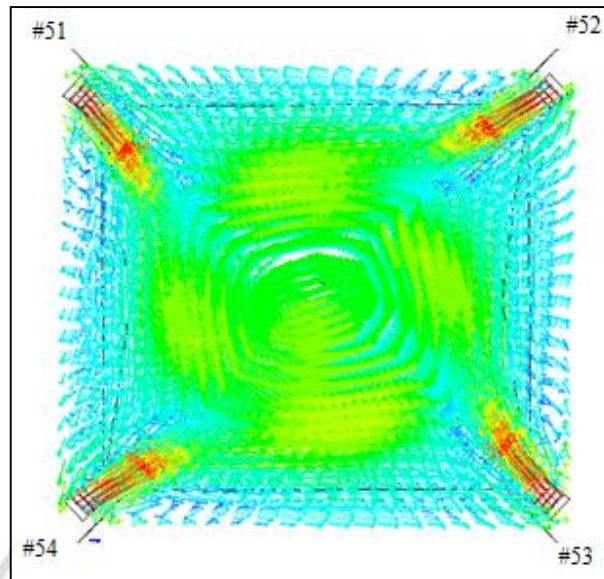


Figure 5.18 Velocity vector in a cross section

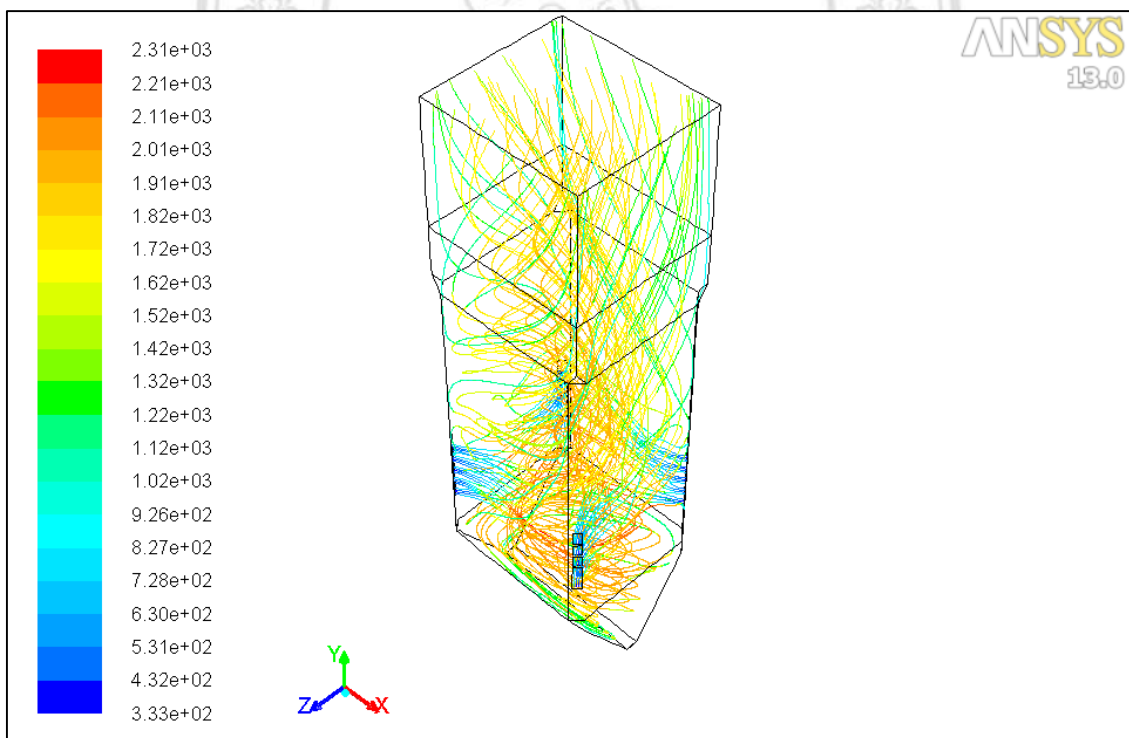


Figure 5.19 Particle trajectory and temperature inside the boiler

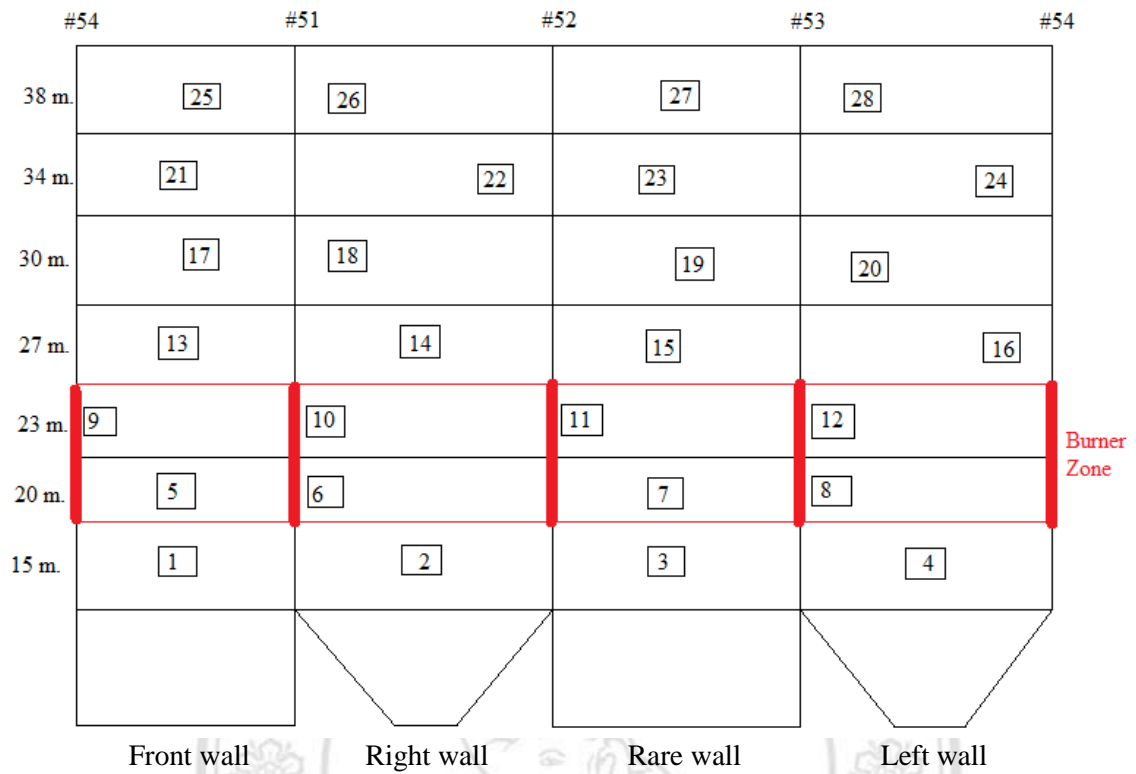


Figure 5.20 The location of the measured heat flux by FACOS system in the Mae Moh boiler

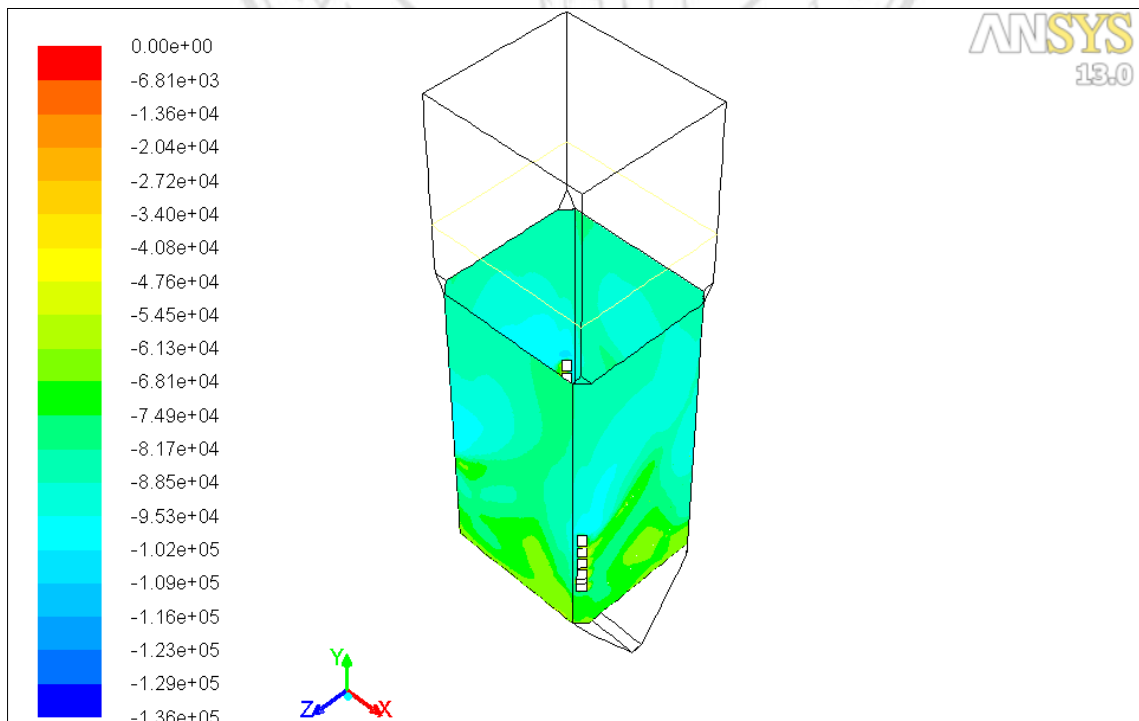


Figure 5.21 Predicted surface heat flux of case study

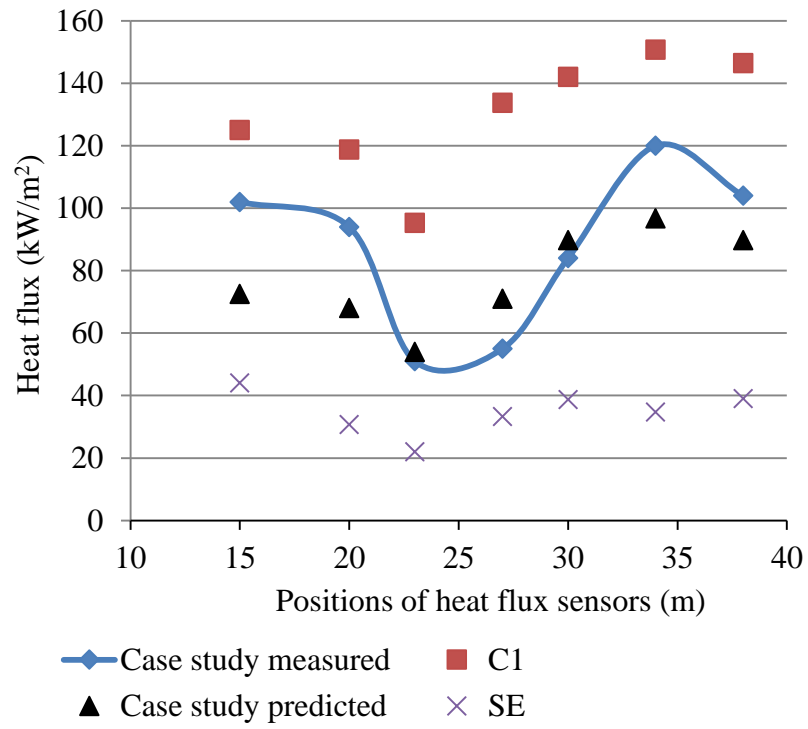


Figure 5.22 Measured and predicted surface heat fluxes of the boiler wall

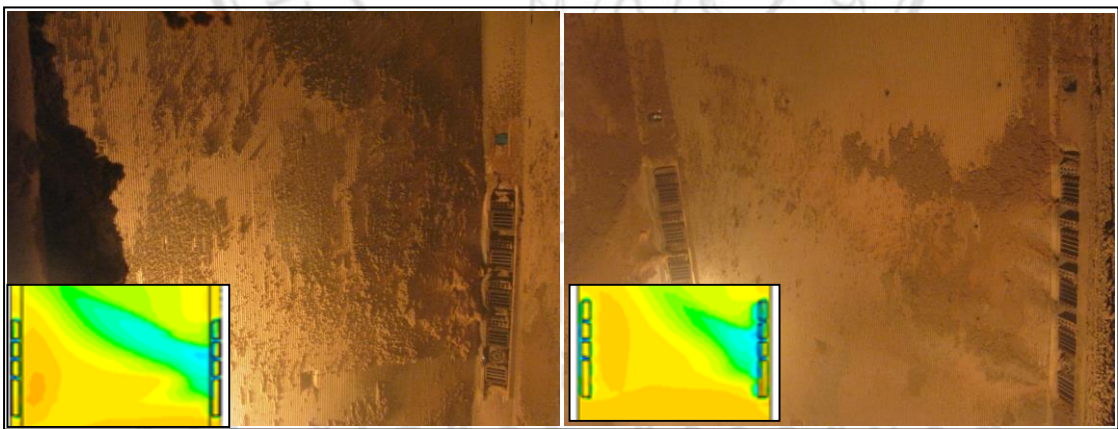


Figure 5.23 Real slag deposition in Mae Moh power plant